Lab on a Chip

Accepted Manuscript

This article can be cited before page numbers have been issued, to do this please use: J. Lee, M. Kim, J. Park and T. Kim, *Lab Chip*, 2016, DOI: 10.1039/C6LC00116E.

ROYAL SOCIETY OF CHEMISTRY

www.rsc.org/loc

View Article Online
DOI: 10.1039/C6LC00116E

Self-assembled Particle Membranes for *In situ* Concentration and Chemostat-like Cultivation of Microorganisms on a Chip

Jongwan Lee[1], Minseok Kim[1], Jungyul Park[2] and Taesung Kim[1,3*]

[1]Department of Mechanical Engineering, Ulsan National Institute of Science and Technology (UNIST), 50 UNIST-gil, Ulsan 44919, Republic of Korea

[2]Department of Mechanical Engineering, Sogang University, Sinsudong, Mapogu, Seoul 04107, Republic of Korea

[3]Department of Biomedical Engineering, Ulsan National Institute of Science and Technology (UNIST), 50 UNIST-gil, Ulsan 44919, Republic of Korea

***CORRESPONDING AUTHOR:**

Taesung Kim
Department of Mechanical Engineering
Ulsan National Institute of Science and Technology (UNIST)
50 UNIST-gil, Ulsan 44919, Republic of Korea
E-mail: tskim@unist.ac.kr
Tel: +82-52-217-2313
Fax: +82-52-217-2409

View Article Online
DOI: 10.1039/C6LC00116E

ABSTRACT

Recently, microparticles have been used as nanoporous membranes in microfluidic devices, contributing to various bioassays on a chip. Here, we report a self-assembled particle membrane (SAPM) integrated microfluidic device that concentrates particles into an aimed microchamber array by using evaporation-driven capillary forces, and manipulates the chemical environment of the microchamber array by sequentially introducing different solutions. We demonstrate that the SAPM-integrated microchamber array can concentrate microparticles and microbial cells up to 120-fold for 2 h and 35-fold for 1 h, respectively, resulting in remarkably high concentration factors. Additionally, we demonstrated that the microchamber array has high potential as a chemostat-like bioreactor because it can actively manipulate the initial seeding number of bacterial cells and continuously supply and sequentially switch fresh nutrients to them. As an example of various applications, the chemostat-like bioreactor was used as a microbial biosensor platform that enabled microbial sensor cells to respond more efficiently and rapidly to external stimuli, such as heavy metal ions. This was possible by almost eliminating the initial lag phase that dramatically shortened the whole assay time. Notably, the SAPM-integrated microchamber array not only facilitates various bioassays on a chip but also provides unprecedented experimental platforms to study microorganisms in a simple and convenient manner.

Keywords: microbioreactor, self-assembled particle membrane, concentration, microbial biosensor platform

View Article Online
DOI: 10.1039/C6LC00116E

INTRODUCTION

Microfluidics showing the ability to manipulate fluids at the nano- or picoliter scales have been considered as an appropriate approach for clinical diagnosis [1], biological assay [2, 3], and (bio-)chemical analysis [4, 5]. In particular, microfluidic devices have been widely used in observation, detection, and analysis of cellular responses under various experimental conditions involving toxicants [6], specific molecules [7] or other microorganism communities [8]. Such microfluidic devices enabled researchers to study microorganisms/cells at the single cell level [9, 10], and made it possible to investigate ensemble averaged cellular responses in a qualitative and/or quantitative manner [11, 12]. For both the cases, it is essential to trap or accumulate cells at a certain location in a microfluidic device to interrogate cellular responses with high accuracy and high reliability [13, 14].

To date, many microfluidic devices have successfully concentrated various bacterial cells on a chip [15-18]. As an active approach, electrokinetics was adopted to freely manipulate or continuously focus the population of cells in a microfluidic device by using dielectrophoresis [15], ion concentration polarization [16], and isoelectric focusing [17]. However, electrokinetic approaches rely on external electric power sources, probably affecting target samples and making the microfluidic device less portable, and they require the integration of microfabricated electrodes with the device, causing complexity and additional labor and time. In contrast, a passive approach was demonstrated that utilized both intrinsic cellular motility and microfabricated structures to guide cells and then concentrated them at a desired location. This approach is very simple and does not harm cells, but is effective only for motile cells [18].

As a compromising approach, evaporation-assisted cell-concentrating devices were introduced [19, 20] with the following advantages: they require no external energy sources; provide an active approach by adjusting evaporation rates; do not harm target cells; and are free from the motility of

View Article Online
DOI: 10.1039/C6LC00116E

microorganisms. Therefore, it seems that they take the advantages of the previous approaches. Notably, nanoporous membranes or structures play a key role in selectively transferring the liquid in the solution, but prevent samples from being removed. Generally, a commercial nanofibrous membrane with fine and uniform pores is integrated into a microfluidic device so cells in a suspension solution can be concentrated by vaporizing the liquid (i.e., evaporation) through the membrane pores [19]. Similarly, micropillar structures fabricated by standard photolithography techniques have been used for the same purpose as the membrane, resulting in the concentration of target samples ranging from 100 nm to 1 μm [20]. However, membrane-integrated microfluidic devices show weaknesses in robustness, repeatability, fluid sealing, etc. Batch-processed micropillar structures were developed to resolve some of these problems. However, microstructures (> 1 μm pores) have a disadvantage as the air-liquid interfaces can be easily broken by high pressure or strong convection, although they are more easily produced than nanostructures (< 1 μm pores) that are inappropriate for large-scale membranes in terms of fabrication cost and throughput. Therefore, it is necessary to develop a simple and robust fabrication method for integrating either membranes or structures with tunable porosities and microfluidic devices, utilizing evaporation efficiently for cell concentration on a chip.

In our previous work, microparticles were employed as an elementary building block to create nanoporous membranes in a microfluidic device [21, 22]. This method relies on the self-assembly of microparticles so that self-assembled particle membranes (SAPMs) show several strengths over thin-film- or microstructure-based membranes. It is advantageous to fabricate SAPMs at multiple desired locations in a microfluidic device by designing a multi-level microchannel network. The SAPM porosities are easily tunable using different particle diameters, ranging from several microns to several tens of nanometers. Since SAPMs provide stable and robust air-liquid interfaces, even in the presence of strong gas or liquid convection, the combination of SAPMs and evaporation-driven microfluidic

View Article Online
DOI: 10.1039/C6LC00116E

devices is possibly useful to concentrate target cells on a chip [23]. In the present study, we presented an SAPM-integrated microfluidic device with a microchamber array and described its fabrication method. We experimentally characterized the concentration factors of the SAPM-integrated microchamber array device using microparticles and microorganisms to theoretically analyze the concentration mechanism. We also showed that the device provides a chemostat-like cell culture environment by continuously supplying a fresh nutrient solution with concentrated cells and preventing the concentrated cells from relocating out of the microchamber array through the SAPM. We further demonstrated that the device allows the control of the number of concentrated cells (i.e., the initial seeding number) in the microchamber array, and investigated the cellular growth behavior in a high-throughput manner. Lastly, we showed that the microchamber array device functions as a microbial biosensor platform to demonstrate the versatile applications of the device.

EXPERIMENTAL

Reagents and materials

Polystyrene particles with a diameter of 1 μm were mainly used to visualize SAPM formation and characterize particle and cell concentration factors. Since 1-μm particles theoretically give rise to a pore size of about 410 nm when forming an SAPM, they were chosen to concentrate 1-μm-spherical particles and 1 μm by 2 μm rod-shaped bacterial cells. Rhodamine-labeled particles (F-13082, Life Technology Korea LLC, Seoul, Korea) of 1 mM (ca. 5×10^9 beads/mL) were prepared in a mixture of ethanol (35 wt%) and distilled water (DW), which shortened the self-assembly time of particles by increasing the evaporation rate of the solvent. The same particle suspension (1 mM) was further diluted with DW for the characterization of concentration factors (i.e., 100 μM, corresponding to 5×10^8 beads/mL). After the characterization of the SAPM formation and the concentration factors using

View Article Online
DOI: 10.1039/C6LC00116E

fluorescence particles, carboxylate and unlabeled polystyrene particles 1 μm in diameter (08226-15, PolySciences Inc., Warrington, PA, USA) were used for SAPM formation to eliminate any fluorescence interference with the components of the concentrated samples such as particles and bacterial cells. Fluorinated oil (FC-40, Sigma-Aldrich, St. Louis, MO, USA) was used to compartmentalize a fluid/microchamber array and prevent its evaporation. PDMS (Sylgard 184, Dow Corning Corp., Midland, MI, USA) was used to fabricate microfluidic devices.

Fabrication and operation of microfluidic devices

The microfluidic device was fabricated using standard photolithography as shown in Figure S1 (Supplementary Information). A negative photoresist (SU-8 2010, Microchem Co., Westborough, MA, USA) was spin-coated on a silicon wafer (10 μm) and then soft-baked. After exposure to UV light using a photomask and mask aligner (MA6, SussMicroTec, Garching, Germany), a photoresist (SU-8 2050, Microchem Co.) was additionally spin-coated as the 2nd layer (50 μm), and subsequently soft-baked. After exposure to UV light using a second photomask and the same mask aligner, the processed silicon wafer was soaked in developer solution to remove the unexposed photoresist and create a multi-level master mold. Subsequently, the surface of the master mold was functionalized with trichloro(3,3,3-trifluoropropyl)silane (452807, Sigma-Aldrich). A PDMS mortar with a 10:1 mixing ratio of base to curing agent was degassed for 30 min in a vacuum jar before the soft-lithography process. The PDMS mixture was poured on the master mold and then cured in an 80°C oven. A replicated PDMS device was detached from the master mold and then attached to a transparent glass substrate using oxygen plasma under 10 sccm of oxygen and 10 W for 1 s (Cute-MP, Femto Science, Gyeonggi-do, Korea). All fluids were injected through a polymeric tube using a syringe pump, and the flow rate was primarily controlled at approximately 500 nL/min.

Preparation of bacterial cells

View Article Online
DOI: 10.1039/C6LC00116E

Several strains of *Escherichia coli* containing different plasmids were used in the present study. The MG1655 strain harboring the pTKU4-2 plasmid is motile and constitutively expresses green fluorescent protein (GFP). The DH10B strain harboring the pTKU4-65 plasmid is immotile and constitutively expresses red fluorescent protein (RFP). Two microbial sensor cells were used to detect heavy metal ions. HK621 sensor cells harboring the pHK194 plasmid expressed GFP in the presence of Pb^{2+}, whereas HK622 sensor cells harboring the pHK200 plasmid expressed GFP in the presence of Cd^{2+} [24]. For all experiments, a single colony was obtained from a Luria Broth (LB) agar plate using a pipette tip and placed in a test tube containing 5 mL LB broth media and 5 μL antibiotics (ampicillin). The test tube was placed in a rotary shaking incubator (37°C) at 200 rpm for 12 h. The resulting OD_{600} reached approximately 2 (ca. 1.6×10^9 cells/mL). To enhance cell motility, Tryptone Broth (TB) media containing the same antibiotics was used rather than LB media, because TB media increases the motility of bacterial cells [25]. All chemicals for cell preparation were purchased from Sigma-Aldrich.

Experimental setup and data analysis

An UV spectrophotometer (Libra S22, Biochrom Ltd., Cambridge, UK) was used to measure the optical densities of the bacterial cells. An inverted fluorescence microscope (IX71, Olympus Corp., Tokyo, Japan) equipped with a CCD camera (Clara Interline CCD, Andor Technology Ltd., Belfast, UK) was used to observe and analyze particles and cells. A cell incubation system (Chamlide TC, Live Cell Instrument, Seoul, Korea) was equipped on the microscope stage to maintain the temperature and humidity of the microfluidic device at 37°C and 60%, respectively. During all experiments, images were captured using imaging software (MetaMorph v7.8.10.0, Molecular Devices, Sunnyvale, CA, USA). Fluorescence intensities of the images were quantitatively analyzed using Image J (1.45s, National Institutes of Health, Bethesda, MD, USA). To determine the particle and cell concentration factors, the fluorescence intensities of Rhodamine-labeled particles and GFP- or RFP-expressing

View Article Online
DOI: 10.1039/C6LC00116E

bacterial cells in the triangular microchamber were obtained and then normalized with those of the same particles and cells in the main loading channel using the same areas or pixel numbers. The normalized fluorescence intensities were drawn as graphs using Origin8 software (v8.0951, OriginLab Corp., Northampton, MA, USA). Fluorescence intensity from the background signal was subtracted from all quantitative analyses. Scanning electron microscope (SEM) images were taken when necessary (SU-8220, Hitachi Ltd., Tokyo, Japan) by sputtering platinum on the surfaces of PDMS devices.

RESULTS AND DISCUSSION

Formation and integration of SAPMs

Figure 1 shows the fabrication process for an SAPM-integrated microfluidic device in which the channel network was filled with a food dye solution. As shown in Figure 1(a), the device consists of two main channels (i.e., Channel-A and -B) for solution loading, triangular microchamber arrays for concentration, culture, and analysis of bacterial cells, and low-level interfaces connecting Channel-A and the triangular microchamber arrays. Figure 1(b) illustrates the integration of SAPMs at a microchamber array. A particle suspension solution loaded along Channel-A flowed through the low-level channel, but stopped at the interface because capillary forces were caused by the expanding channel geometry [26]. Therefore, SAPMs were formed in parallel in the microchamber array. Figure 1(c) shows a series of bright field and fluorescence images during SAPM fabrication; particles were fluorescently labeled for visualization. Channel-A was filled with a particle suspension solution while Channel-B was empty at $t = 0$. The particles were continuously self-assembled at the interface over time. Self-assembly started at the narrow edge of the low-level channel and proceeded continuously along the wide-edge side until the low-level channel was completely packed. After 3 h of self-assembly, we flushed Channel-A with air and found that an SAPM had been successfully formed (Figure S2,

View Article Online
DOI: 10.1039/C6LC00116E

Supplementary Information). We tested the SAPM fabrication method for various channel geometries using labeled or unlabeled carboxylate particles and confirmed that the same method could be directly applied to the formation of SAPMs in various microchamber arrays (Figure S3, Supplementary Information).

Particle and cell concentrations

We formed SAPMs using unlabeled microparticles and conducted concentration experiments using fluorescently labeled microparticles. First, we filled the concentration chambers with DW through the bottom channel and then flushed it with a particle suspension solution. Figure 2 shows the bright and fluorescence images during concentration, where fluorescently labeled particles were drawn towards the SAPM and then continuously accumulated at the interface. This is because water molecules evaporated out to the top channel (Channel-A) through the SAPM, enabling particles to move along the surrounding fluid. As shown in Figures 2(a) and (b), the high temperature led to a rapid concentration of the microparticles because the evaporation of water through the SAPM increased at higher temperatures. Figure 2(c) shows the quantified concentration factors and the control experiment, where no particle concentration was observed; slight concentration was possibly caused by Brownian motion [27] (Figure S4(a), Supplementary Information). After 100 min, the concentration factors reached 7 (25°C) and 12 (40°C) compared to the control experiment. Water evaporation was completely blocked by loading oil in Channel-A for negative control experiments in the present study as otherwise noted. Figures 2(d) and (e) show the effect of forced convection on the concentration factors at the same temperature conditions as described above. For forced convection, we used compressed N_2 gas where the inlet pressure was approximately 5 kPa, corresponding to flowrate of 5×10^{-5} m^3/min. Many particles rapidly accumulated at the SAPM interface (refer to Supplementary Movie). Figure 2(f) shows the concentration factors reaching 120 and 110, depending on the

View Article Online
DOI: 10.1039/C6LC00116E

temperature. Therefore, the concentration factors were actively manipulated by controlling the temperature and/or convection, ranging from several- to a hundred-fold within 2 h. This is useful to adjust the initial seeding number of cells in the microchamber array.

A similar experiment was repeated using two bacterial strains: one was motile (MG1655) and engineered to produce GFP, and the other was immotile (DH10B) and engineered to produce RFP. In a similar manner as Figure 2, TB media was first loaded into the bottom channel so that the chamber was filled with media. Second, the bottom channel was flushed with a cell suspension solution and then forced convection was applied by flowing N_2 gas through the top channel. As shown in Figures 3(a) and (b), cells in the bottom channel were drawn toward and then accumulated at the SAPM interface over time. However, when evaporation was almost completely suppressed by filling the channel with oil, only a minimal fluorescence signal was detected, implying that no concentration occurred (Figures S4(b) and (c), Supplementary Information). As shown in Figure 3(c), the quantified concentration factors show that bacterial cells were highly accumulated in the microchamber than that of the control experiment. Interestingly, there was no significant difference between motile and immotile bacterial cells. From this result, it is conjectured that cell motility is negligible because the evaporation-driven capillary forces inside the SAPM are more dominant.

It is worthy to discuss why the concentration factors are different between the particles and the cells. Since the concentration factors are linearly proportional to the multiplication of the concentration rate and time, we analyzed the concentration rates (slopes) of the particles (1.18 Au/min) and the cells (0.46 Au/min) at the same time point and found that the former is 2.6 times greater than the latter as shown in Figures 2(f) and Figure 3(c). As shown in Figure 4, we directly measured the moving velocities of the particles and cells at the same concentration conditions by tracing 10 individual samples, respectively. Figures 4(a) and (c) show the snapshots of 10 particles and 10 cells (MG1655)

View Article Online
DOI: 10.1039/C6LC00116E

near the entrance of the microchamber at t = 0 sec and t = 3 s. All the particles and cells migrated toward the SAPM, accumulating over time. Figures 4(b) and (d) show the pathlines (traces) of the particles and the cells at 0.5 s intervals so that the velocities of the particles and cells could be calculated as 35.4 and 13.0 μm/s on average, respectively. Interestingly, the velocity ratio of particles to cells was V_p/V_c = 2.7, which is similar to the ratio of the concentration rates (slopes).

In theory, the different concentration factors can be explained by the characteristic length of 3D objects in low Reynolds flows where the viscous drag (frictional) forces of small particles can be estimated by using the following equation [28, 29]:

$$F_d = C_d V$$

where C_d is the drag coefficient of an object and V its moving velocity in a stationary fluid. For example, the drag coefficient of spherical particles is known from Stokes' law:

$$C_{d\_p} = 6\pi\mu r$$

However, for cylindrical shapes, the drag coefficient is expressed as follows:

$$C_{d\_c} = \frac{2\pi\mu L}{\ln(L/2r) - 0.20}$$

where μ, r and L are the dynamic viscosity of fluid ($\mu = 0.89 \times 10^{-3}$ Pa·s for water), the radius, and the length of cylindrical cells (i.e., r = 0.5 μm and L = 2 μm), respectively. Therefore, the drag coefficient ratio of the 1-μm by 2-μm cells to the 1-μm-particles is C_{d_c}/C_{d_p} = 2.7. Additionally, we assumed that evaporation imposed the same viscous drag forces (F_d) on the particles and cells and the specific gravities of the particles and cells were almost the same as the fluid (water). Therefore, the resulting velocity ratio agreed well with the drag coefficient ratio; that is $V_p/V_c = C_{d\_c}/C_{d\_p}$. In conclusion, the ratio was similar to the ratio of the concentration rates, and therefore, the experimental results were

View Article Online
DOI: 10.1039/C6LC00116E

well supported by the theoretical analysis. We noted that advection was dominant, and diffusion was negligible during the concentration process; the Peclet number was estimated to be about 10^4 [30].

Applications to chemostat-like microbioreactor

We tested cell growth in the microfluidic device using three initial seeding numbers of cells in the microchamber, which were easily controlled by regulating the density of the cell suspension solution to load (e.g., OD_{600} = 0.6) and then varying the concentration time according to the previous result in Figure 3(c). As shown in Figure 5(a), three initial seeding numbers of the cells, such as $n_i < 10$, n_i = 400, and n_i = 40,000, were concentrated in the microchambers by adjusting the concentration durations by < 5 s, 4 min, and 45 min, respectively. Next, oil was loaded into the bottom channel for compartmentalization of the microchamber arrays while LB rich media was continuously supplied to the top channel for chemostat-like culture. Cell growth was indirectly quantified by measuring the fluorescence intensities of the cells as shown in Figure 5(b). For the highest initial cell number (i.e., n_i = 40,000 cells), as soon as LB rich media was supplied, the fluorescence intensities increased rapidly, immediately undergoing a log phase without a lag phase. In approximately 11 h, the microchamber appeared to be completely filled with cells with an OD_{600} of approximately 200. It is possible that additional cell division could not occur because there was no additional space in the microchamber, although the chemical conditions for cell division were well maintained. In contrast, for the lower initial cell numbers (i.e., < 10 and 400 cells), it was difficult to detect fluorescence signals from the cells at the early stage. The lag phase continued for about 4 and 11 h, respectively, and then both growth curves showed a log phase. As the initial seeding numbers of the cells increased, the slopes of the fluorescence intensities over time became steeper; that is 1,798 au/h for n_i = 40,000, 1,226 au/h for n_i = 400, and 1,287 for $n_i < 10$ cells, respectively. From these results, we can see that the initial seeding numbers of the cells shortened the lag phase and manipulated the slopes of the log phases,

View Article Online
DOI: 10.1039/C6LC00116E

demonstrating the ability to enhance the response time and sensitivity of microbial biosensors [24]. When the microchamber was completely filled with cells, the resulting OD_{600} apparently exceeded 200 (1.6×10^{11} cells/mL), which cannot be typically achieved in a conventional batch-feed mode culture. It is noted again that the highest initial seeding numbers of the cells facilitated rapid bacterial assays on a chip by significantly reducing the lag phase, showing high potential for use as microfluidic bioreactor.

We employed two microbial biosensors and further utilized the device as a microbial biosensor platform: pHK194/HK621 and pHK200/HK622 for Pb^{2+} and Cd^{2+} detection, respectively. Three different initial seeding numbers of the biosensor cells were tested concurrently on a chip as shown in Figures 6(a) and (c); approximately $n_i < 10$, $n_i = 400$, and $n_i = 40{,}000$ were tested as shown in Figure S5 in Supplementary Information. Similarly to the cellular growth experiment in Figure 5, the initial seeding numbers of the cells significantly affected the cellular responses. In the presence of the same concentration of target heavy metal ions (i.e., 20 μM of Pb^{2+} and 20 μM of Cd^{2+}, respectively), the response times of the fluorescence intensities depended highly on the initial seeding numbers of the biosensor cells. The higher the initial seeding numbers, the stronger and earlier fluorescence intensities were detected. Interestingly, the microchambers appeared to be completely filled with cells and each cell could produce GFP at its maximum expression level.

Figures 6(b) and (d) show the quantified fluorescence intensities of the microbial biosensor cells, which were measured in parallel on a chip. For both the microbial biosensor cells, the highest initial seeding number showed more rapid responses and steeper slopes than the low initial seeding numbers. For example, the highest initial seeding number of HK621 cells showed *in situ* fluorescence responses as soon as target heavy metal ions (Pb^{2+}) were loaded, whereas the lowest initial seeding number required approximately 15 h to pass over the log phase and then showed the fluorescence responses (Figure 6(b)). In contrast, the fluorescence intensities of HK622 cells in the presence of Cd^{2+} ions

View Article Online
DOI: 10.1039/C6LC00116E

showed different behavior (Figure 6(d)). In particular, for the low initial seeding numbers, it took much longer for the cells to show a log phase (about 30 h). This could be attributed to the toxicity of Cd^{2+} ions to cell growth. Importantly, the high initial seeding number resulted in steeper slopes of the fluorescence intensities, implying that the sensitivity can be improved by the platform; 2,156 au/h (n_i = 40,000) *vs*. 1,997 (n_i < 10) and 1,984 au/h (n_i = 400) for HK621 while 308 au/h (n_i = 40,000) *vs*. 194 (n_i < 10) and 190 au/h (n_i = 400) for HK622. Negative control groups showed much weaker fluorescence intensities than the experimental groups (Figure S6 in Supplementary Information).

In summary, it is obvious that the initial seeding number and the chemostat-like continuous culture environment shortened the lag phase and steepened the slopes, resulting in enhanced biosensor performance in terms of response time and sensitivity. Therefore, the ability to concentrate cells into a desired microchamber array played a crucial role in enhancing the performance of the microbial biosensor cells, indicating that the SAPM-integrated microfluidic device could be used as a microbial biosensor platform. It is also possible to expand the SAPM-integrated microfluidic device for use as a multiplex microbial biosensor platform because the microchamber array with SAPMs can be easily integrated with other microfluidic components such as a micromixer and a concentration generator as illustrated in Figure S7 in Supplementary Information. A wide range of concentrations of target analytes could be generated using a concentration generator and various microbial biosensor cells could be compartmentalized in the microchamber array, making it easier to develop a multiplex microbial biosensor platform.

CONCLUSIONS

We developed an SAPM-integrated microfluidic device that made it possible to concentrate particles/cells by using evaporation-driven capillary forces through the SAPM. The resulting concentration factors ranged from 100 to 120 for microparticles within 2 h and were approximately 30

View Article Online
DOI: 10.1039/C6LC00116E

for motile and immotile bacterial cells within 1 h. We demonstrated that the microfluidic device can compartmentalize the concentrated cells by simply switching fluids (e.g., oil and aqueous solution) and then culture bacterial cells in a chemostat-like manner. We found that high initial seeding cell numbers in a microchamber array, which was easily adjusted by manipulating the concentration time of target cells, substantially shortened or almost eliminated the lag phase. As an example of applications, we used the device as a microbial biosensor platform that reduced the response time by about 10 to 20 h and enhanced the sensitivity of the microbial biosensors in the detection of heavy metal ions. Hence, it is expected that the SAPM-integrated microfluidic device would be a versatile platform for *in situ* concentration and rapid biological and/or chemical assays of various biosamples in a high-throughput manner.

ACKNOWLEDGEMENTS

This work was supported by the 2015 Research Fund (1.150033.01) of UNIST (Ulsan National Institute of Science and Technology), a National Research Foundation of Korea (NRF) grant funded by the Korean government (MSIP) (NRF-2014R1A2A1A10050431), and a grant from the Next-Generation BioGreen 21 Program (SSAC, PJ01118601), Rural Development Administration, Republic of Korea.

View Article Online
DOI: 10.1039/C6LC00116E

REFERENCES

1. Yager, P., et al., *Microfluidic diagnostic technologies for global public health.* Nature, 2006. **442**(7101): p. 412-418.

2. Balagaddé, F.K., et al., *Long-term monitoring of bacteria undergoing programmed population control in a microchemostat.* Science, 2005. **309**(5731): p. 137-140.

3. Groisman, A., et al., *A microfluidic chemostat for experiments with bacterial and yeast cells.* Nature methods, 2005. **2**(9): p. 685-689.

4. Martinez, A.W., S.T. Phillips, and G.M. Whitesides, *Three-dimensional microfluidic devices fabricated in layered paper and tape.* Proceedings of the National Academy of Sciences, 2008. **105**(50): p. 19606-19611.

5. Whitesides, G.M., *The origins and the future of microfluidics.* Nature, 2006. **442**(7101): p. 368-373.

6. Biran, I., et al., *Optical imaging fiber-based live bacterial cell array biosensor.* Analytical Biochemistry, 2003. **315**(1): p. 106-113.

7. Rothert, A., et al., *Whole-cell-reporter-gene-based biosensing systems on a compact disk microfluidics platform.* Analytical biochemistry, 2005. **342**(1): p. 11-19.

8. Lee, S.H., et al., *Capillary based patterning of cellular communities in laterally open channels.* Analytical chemistry, 2010. **82**(7): p. 2900-2906.

9. Uhlendorf, J., et al., *Long-term model predictive control of gene expression at the population and single-cell levels.* Proceedings of the National Academy of Sciences, 2012. **109**(35): p. 14271-14276.

10. Taniguchi, Y., et al., *Quantifying E. coli proteome and transcriptome with single-molecule sensitivity in single cells.* Science, 2010. **329**(5991): p. 533-538.

11. Mohan, R., et al., *A multiplexed microfluidic platform for rapid antibiotic susceptibility testing.* Biosensors and Bioelectronics, 2013. **49**: p. 118-125.

12. Dai, J., et al., *Charting microbial phenotypes in multiplex nanoliter batch bioreactors.* Analytical chemistry, 2013. **85**(12): p. 5892-5899.

13. Sun, P., et al., *High-throughput microfluidic system for long-term bacterial colony monitoring and antibiotic testing in zero-flow environments.* Biosensors and Bioelectronics, 2011. **26**(5): p. 1993-1999.

14. Reyes, D.R., et al., *Micro total analysis systems. 1. Introduction, theory, and technology.* Analytical chemistry, 2002. **74**(12): p. 2623-2636.

15. Lapizco-Encinas, B.H., et al., *Insulator-based dielectrophoresis for the selective concentration and separation of live bacteria in water.* Electrophoresis, 2004. **25**(10-11): p. 1695-1704.

16. Kim, M., M. Jia, and T. Kim, *Ion concentration polarization in a single and open microchannel induced by a surface-patterned perm-selective film.* Analyst, 2013. **138**(5): p. 1370-1378.

17. Cabrera, C.R. and P. Yager, *Continuous concentration of bacteria in a microfluidic flow cell using electrokinetic techniques.* Electrophoresis, 2001. **22**(2): p. 355-362.

18. Hulme, S.E., et al., *Using ratchets and sorters to fractionate motile cells of Escherichia coli by length.* Lab on a Chip, 2008. **8**(11): p. 1888-1895.

View Article Online
DOI: 10.1039/C6LC00116E

19. Zhang, J.Y., et al., *Rapid point-of-care concentration of bacteria in a disposable microfluidic device using meniscus dragging effect.* Lab on a Chip, 2010. **10**(23): p. 3265-3270.

20. Choi, J.W., et al., *A micropillar array for sample concentration via in-plane evaporation.* Biomicrofluidics, 2014.

21. Choi, E., et al., *Concentration gradient generation of multiple chemicals using spatially controlled self-assembly of particles in microchannels.* Lab on a Chip, 2012. **12**(20): p. 3968-3975.

22. Choi, E., et al., *Tunable reverse electrodialysis microplatform with geometrically controlled self-assembled nanoparticle network.* Lab on a Chip, 2015. **15**(1): p. 168-178.

23. Walker, G.M. and D.J. Beebe, *An evaporation-based microfluidic sample concentration method.* Lab on a Chip, 2002. **2**(2): p. 57-61.

24. Kim, M., et al., *Chemostat-like microfluidic platform for highly sensitive detection of heavy metal ions using microbial biosensors.* Biosensors and Bioelectronics, 2015. **65**: p. 257-264.

25. Kim, M., et al., *Microfluidic device for analyzing preferential chemotaxis and chemoreceptor sensitivity of bacterial cells toward carbon sources.* Analyst, 2011. **136**(16): p. 3238-3243.

26. Lam, P., K.J. Wynne, and G.E. Wnek, *Surface-tension-confined microfluidics.* Langmuir, 2002. **18**(3): p. 948-951.

27. Ounis, H., G. Ahmadi, and J.B. McLaughlin, *Brownian diffusion of submicrometer particles in the viscous sublayer.* Journal of Colloid and Interface Science, 1991. **143**(1): p. 266-277.

28. Tirado, M.M. and J.G. de la Torre, *Translational friction coefficients of rigid, symmetric top macromolecules. Application to circular cylinders.* The Journal of Chemical Physics, 1979. **71**(6): p. 2581-2587.

29. Kim, T., et al., *Nanomechanical model of microtubule translocation in the presence of electric fields.* Biophysical journal, 2008. **94**(10): p. 3880-3892.

30. Nguyen, N.-T. and Z. Wu, *Micromixers—a review.* Journal of Micromechanics and Microengineering, 2005. **15**(2): p. R1.

View Article Online
DOI: 10.1039/C6LC00116E

Figures

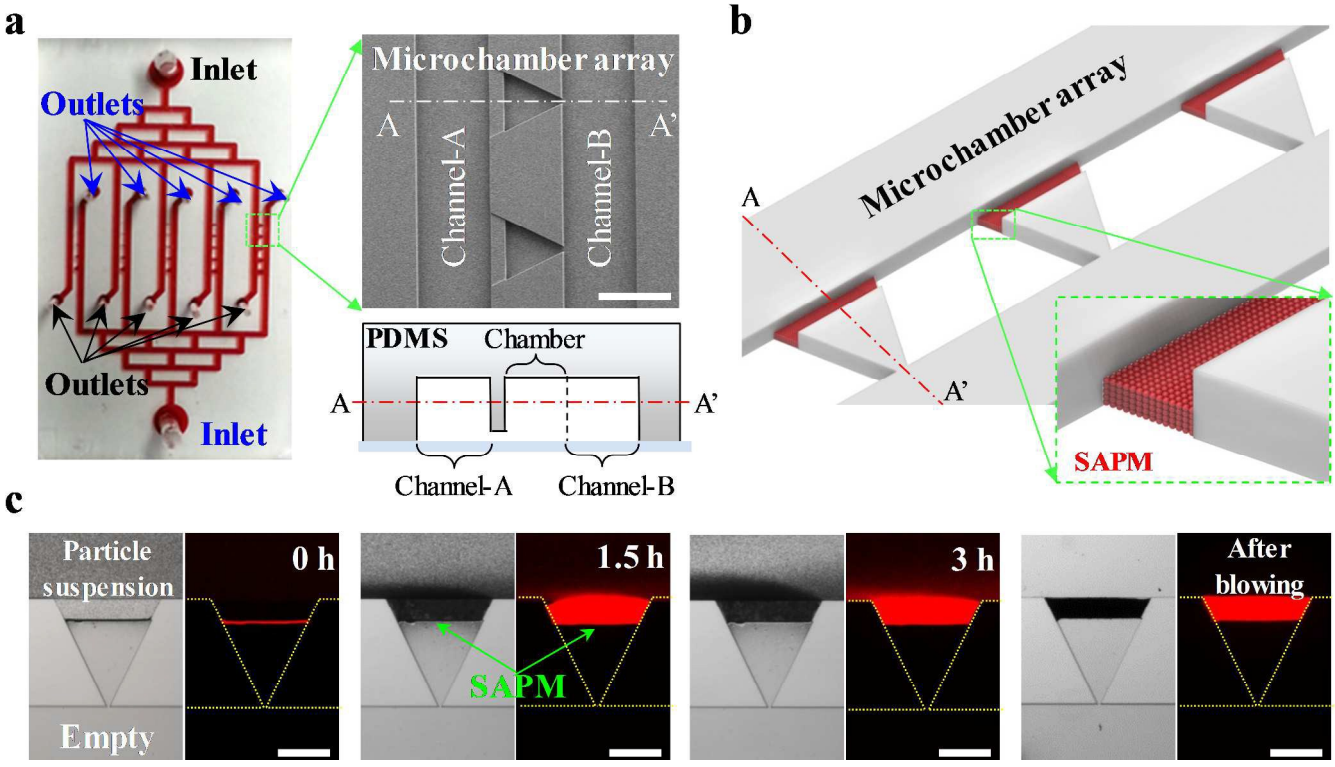

Figure 1. Fabrication of an SAPM-integrated microchamber array. (a) Photograph and SEM image of a microfluidic device of which the channel network consisted of deep (60 μm) and shallow channels (10 μm) (scale bar: 500 μm). (b) Schematic shows integrated SAPMs in the multi-depth microchamber array. (c) Time-lapse microimages of a fabricated SAPM: bright field image (left) and fluorescence (right) (scale bar: 250 μm).

View Article Online
DOI: 10.1039/C6LC00116E

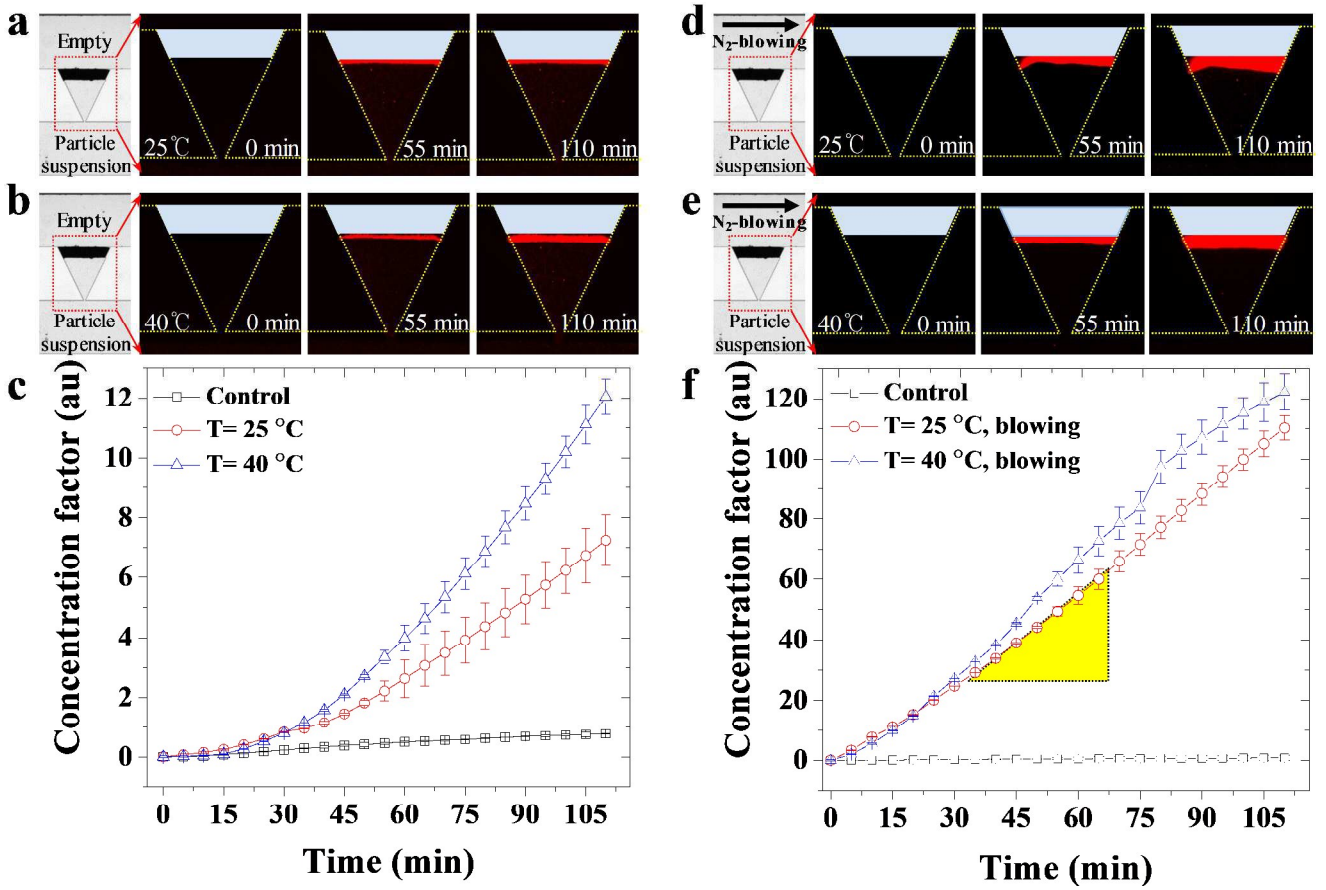

Figure 2. Concentration of microparticles from evaporation through the SAPM. (a)–(b) Concentration of fluorescently-labeled microparticles in the bottom channel under two different temperatures, 25 and 40°C, without convection flow in the top channel. (c) Quantification of concentration factors over time. The air-blowing top channel was filled with oil to completely suppress evaporation (convection flow) for the control experiment. (d)–(e) Repeated concentration experiments with additional air blowing in the top channel. (f) Concentration factors were significantly enhanced under forced convection conditions under the same temperature conditions.

View Article Online
DOI: 10.1039/C6LC00116E

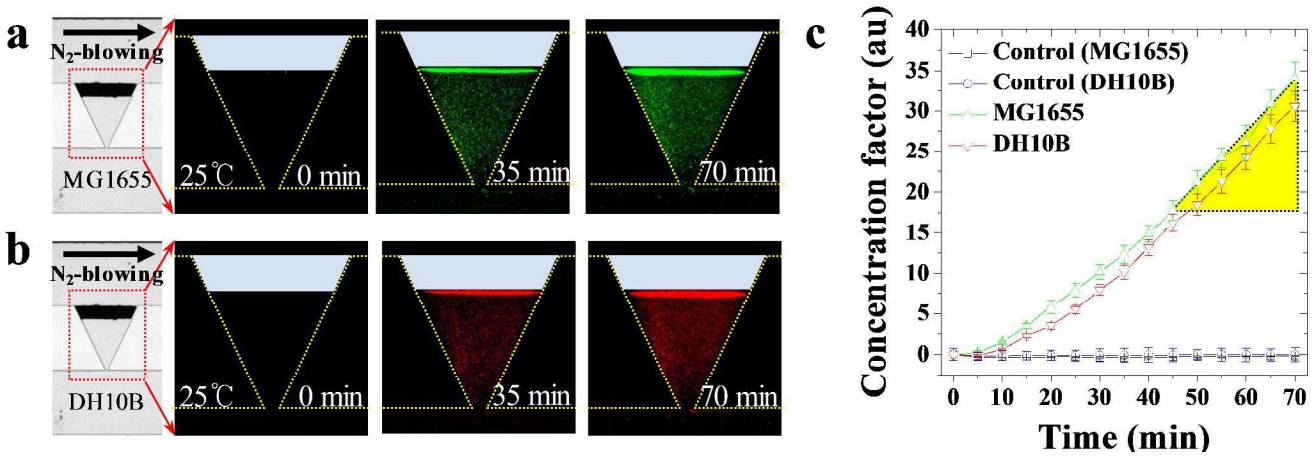

Figure 3 Concentration of bacterial cells under a forced convection condition at room temperature (25°C). (a) Motile cells (MG1655) expressing GFP. (b) Immotile cells (DH10B) expressing RFP. (c) Concentration factors of cells were indirectly quantified using the fluorescence signals of the concentrated cells

View Article Online
DOI: 10.1039/C6LC00116E

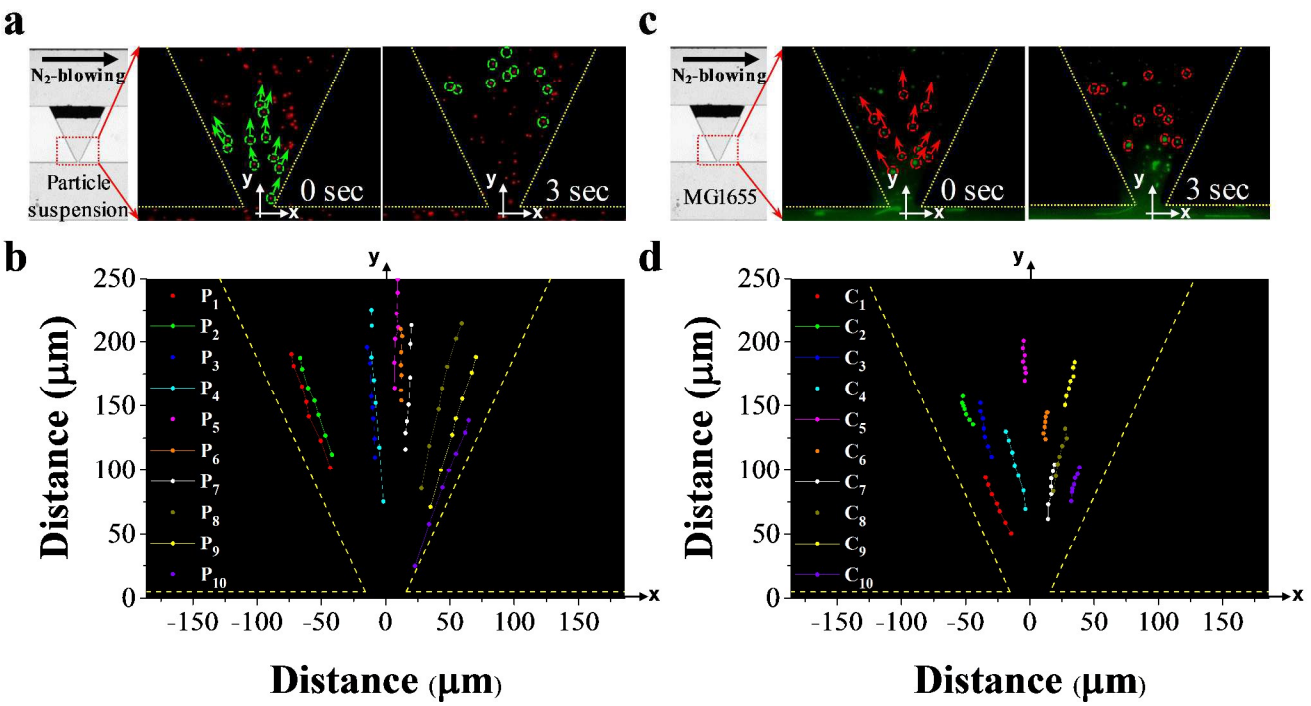

Figure 4 Traces of particles and cells during evaporation-driven concentration. (a)–(b) Locations of 10 individual particles and 10 individual cells at the entrance of the microchamber at t = 0 s and t = 3 s, respectively. (c)–(d) The traces of the particles and cells are indicated at 0.5 s intervals and their moving velocities are about 35.4 μm/s and 13.0 μm/s on average, respectively.

View Article Online
DOI: 10.1039/C6LC00116E

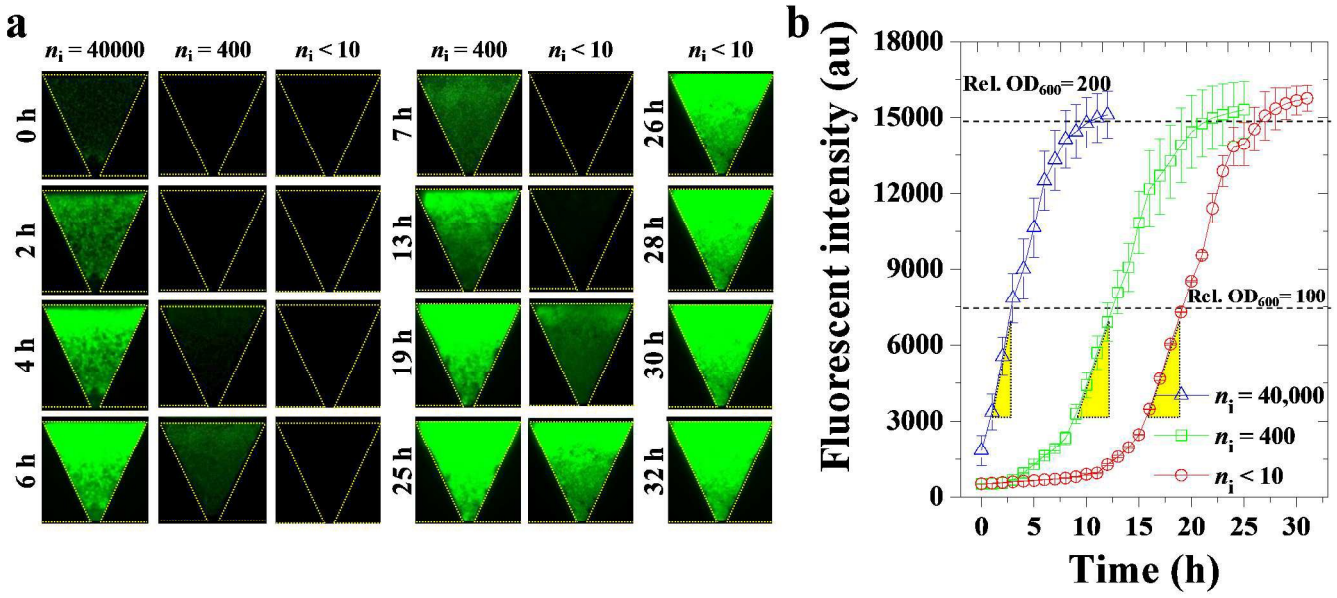

Figure 5 Manipulation of the initial seeding number of cells in the microchamber and chemostat-like cell culture. (a) Three initial seeding numbers of cells were chosen by controlling the concentration time and the OD of cell suspension solutions: several cells (n_i < 10), n_i = 400, and n_i = 40,000 cells for < 5 s 4 min, and 45 min, respectively. (b) Cell growth curves were obtained by using the fluorescence signals of the cells. Two calibrated optical densities (OD_{600} = 100 and 200) were used for reference. The slopes of the log phases are 1,798, 1,226, and 1,287 au/h for n_i = 40,000, n_i = 400, and n_i < 10, respectively.

View Article Online
DOI: 10.1039/C6LC00116E

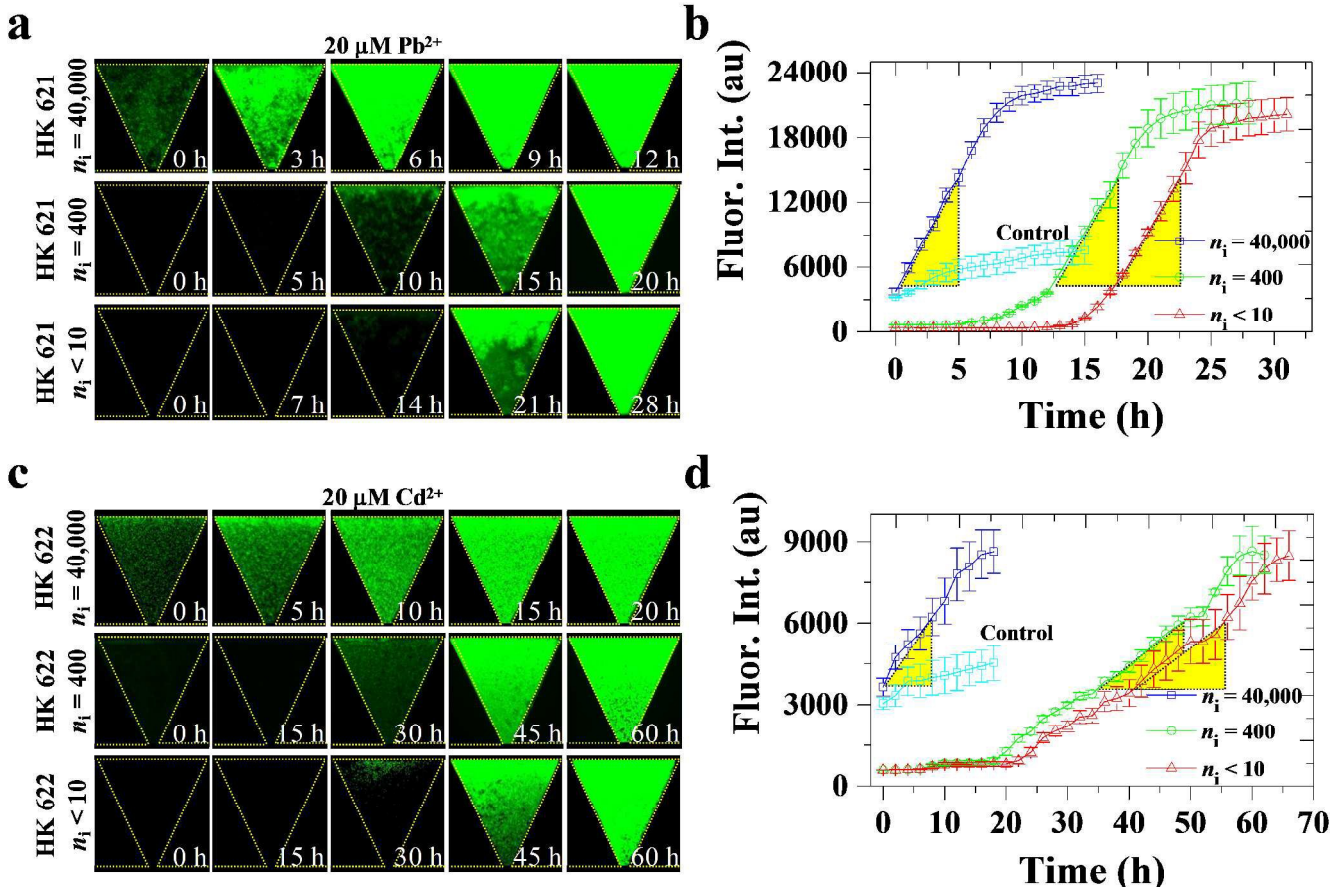

Figure 6 Application of the SAPM-integrated microchamber array to a microbial biosensor platform. (a), (c) Fluorescence responses of microbial biosensor cells, pHK194/HK621 and pHK200/HK622, in the presence of Pb^{2+} (20 μM) and Cd^{2+} (20 μM) ions, respectively. Three initial seeding numbers of cells were tested on a chip in parallel: $n_i < 10$, $n_i = 400$, and $n_i = 40{,}000$. (b), (d) Fluorescence intensities were quantified over time. The slopes of the log phases are 2,156, 1,984, and 1,997 au/h for HK621 cells while those are 308, 190, and 194 au/h for HK621 cells in order of $n_i = 40{,}000$, $n_i = 400$, and $n_i < 10$.